FFEMS Fatigue & Fracture of Engineering Materials & Structures
ORIGINAL CONTRIBUTION
doi: 10.1111/ffe.12547

Fracture toughness and fatigue crack growth rate properties in wire + arc additive manufactured Ti-6Al-4V

X ZHANG[1,2], F MARTINA[1], J DING[1], X WANG[1,2] and SW WILLIAMS[1]

[1]*School of Aerospace, Transport and Manufacturing, Cranfield University, UK,* [2]*Faculty of Engineering, Environment & Computing, Coventry University, UK*

Received Date: 30 July 2016; Accepted Date: 17 October 2016; Published Online:

ABSTRACT This paper presents an experimental investigation of the fracture and fatigue crack growth properties of Ti-6Al-4V produced by the Wire + Arc Additive Manufacture (WAAM®) process. First, fracture toughness was measured for two different orientations with respect to the build direction; the effect of wire oxygen content and build strategy were also evaluated in the light of microstructure examination. Second, fatigue crack growth rates were measured for fully additive manufactured samples, as well as for samples containing an interface between WAAM® and wrought materials. The latter category covers five different scenarios of crack location and orientation with respect to the interface. Fatigue crack growth rates are compared with that of the wrought or WAAM® alone conditions. Crack growth trajectory of these tests is discussed in relation to the microstructure characteristics.

Keywords fatigue crack growth; fracture toughness; microstructure; titanium; wire + arc additive manufacture.

NOMENCLATURE

a	=	Crack length
B	=	Compact tension specimen thickness
K_{IC}	=	Plane-strain fracture toughness
K_Q	=	Conditional fracture toughness value
P_{max}	=	Applied load at fracture
P_Q	=	Conditional load value at fracture determined by ASTM Standard
W	=	Compact tension specimen width
σ_{ys}	=	Material yield strength under tension load

INTRODUCTION

Titanium alloy Ti-6Al-4V (Ti64) has been used in the aerospace and other industries owing to its high specific strength, excellent resistance to fatigue and corrosion, and good performance at elevated temperature. With the increasing use of carbon fibre polymer composites in the airframes, titanium will be increasingly used because of its good compatibility with this material. However, titanium alloys are extremely expensive and very difficult to machine, if compared with other aerospace alloys such as aluminium. Therefore, using the Additive Manufacture (AM) technology to build titanium parts has become very attractive owing to the significant reduction in material waste, machining and tooling cost, manufacturing energy and time to market. Conventional powder bed AM also makes it possible to easily produce complicated parts. However, the cost of material powder is usually particularly high, which affects the overall cost of the process. This drawback is counterbalanced by the reduced material waste. Studies have shown that AM can be an economically and environmentally superior option to the traditional methods of machining from cast or forged billets for production in small batches.[1,2]

The Wire + Arc Additive Manufacture (WAAM®) process works by feeding a wire at controlled rate into an electric or plasma arc, to melt the wire onto a substrate or previously deposited layers. It has found applications

Correspondence: Xiang Zhang. E-mail: xiang.zhang@coventry.ac.uk
WAAM® is a registered trademark of Cranfield University.

in the aerospace and other industrial sectors. The key advantage of wire-based AM if compared with powder-based processes is that WAAM® can produce large, near net shape parts with a deposition of several kilograms per hour, at acceptable cost and in reasonable times.[3,4] Furthermore, wire has much less safety issues. However, as-deposited WAAM® parts have lower accuracy in dimension and surface roughness; therefore, a finish-machining pass is most likely required.[5]

One of the main barriers to the widespread application of AM to aerospace components is the lack of systematic knowledge of mechanical properties, particularly the fatigue and fracture response under service load conditions, which is a key design requirement for product qualification and certification.[2] Changes to the microstructure and tensile residual stresses arising from the manufacturing process have been recognised as the main factors affecting the mechanical properties of AM components.[6–10] While the reductions of structural weight and manufacturing cost have been the main driver to the development of AM technology, durability and damage tolerance capabilities are primary and mandatory requirements for commercial transport. One of the stringent damage tolerance requirements is the capability of predicting fatigue crack growth life and residual strength due to accidental damage. For the AM alloys, this sets two challenges: the development of adequate design tools and predictive models; and the creation of a material property database [e.g. static strength, high cycle fatigue strength, fracture toughness and fatigue crack growth rates (FCGR)]. Because the AM process produces alloys with anisotropic and inhomogeneous properties,[7] different microstructure from the wrought alloy[7,11] and non-uniform residual stresses,[12–15] it is important to investigate the fracture toughness and fatigue crack growth properties for what is effectively a new material form.

To date, most published work reports the static and fatigue strength properties, and only a small number of publications are available on the fracture toughness and FCGR properties of Ti64 fabricated by powder bed or powder feed AM processes, for example via the electron beam melting (EBM),[16] selective laser melting (SLM)[17–23] and laser engineered net shaping (LENS)[24] The value of the apparent fracture toughness of the EBM Ti64 was found to be greater than a reference value in annealed condition,[16] which was attributed to the AM metal's coarse-grained basket-weave microstructure that increases the resistance to fracture. This is also reported for the laser engineered net shaping fabricated Ti64[24] The SLM Ti64 however is found to have lower fracture toughness than the wrought and cast forms.[17,19] In both studies, the authors attributed the inferior fracture toughness in the as-built form to the fine and brittle acicular martensitic structure caused by rapid solidification of the material. In terms of the FCGR, the EBM Ti64 exhibited slower crack growth rates in the Paris law region than that in the wrought condition, in both orientations,[16] whereas FCGR in the SLM Ti64 in the as-built condition was faster in the lower ΔK region (15–30 MPa$\sqrt{m}$) and slower in the higher ΔK region (30–80 MPa$\sqrt{m}$) at load ratio of 0.1.[17] Similar trend was found by another study,[19] in which SLM Ti64 had slower FCGR than the wrought alloy in all three orientations at load ratio 0.1. However, another study recorded faster crack growth rate (by a magnitude) comparing with a reference alloy produced by conventional process.[18] This was also tested at load ratio 0.1. The authors attributed the faster crack growth rate to the process induced porosity and residual stresses. In the same study,[18] for heat-treated and Hot Isostatic Pressing (HIP) treated conditions, crack growth rates are found to be comparable with, or slower than the reference wrought alloy. Computer tomography revealed that porosity was reduced by HIP process to a level below the resolution limit of 22 μm. Therefore, it is worth noting the remarkable effect of post-build heat treatments, such as stress relief annealing or HIP. FCGR is significantly reduced by annealing[21,22] and the threshold value of stress intensity factor (SIF) range is increased[23] There are also work on using heat and mechanical treatments to improve the high cycle fatigue strength in AM build nickel[25] and steel alloys.[26]

Discrepancies in published crack growth rates can also arise from post-build machining. For example, specimens used in the work[17,19] were machined from oversized blocks, for example from 65 × 65 × 5 mm block to C(T) sample of 50 mm wide and 4 mm thick.[19] Conversely, in another work[18] surfaces were left in the as-built condition[20] as the aim was to test the three conditions of as-built, heat-treated and HIP. Therefore, specimens in[18] may have surface roughness and internal defects that might have resulted in greater crack growth rate in the as-built condition. Furthermore, specimen size can also affect the magnitude of residual stress. Study in[12] shows that residual stress is released considerably by machining test samples from a larger piece. Therefore, samples extracted from oversized block in[17,19] may have reduced the residual stress magnitude and surface defects resulting in slower crack growth rates.

In summary, EBM Ti64 has comparable or superior fracture toughness and crack growth rates than wrought condition owing the building at elevated temperature resulting in negligible residual stress. The as-built SLM has poorer fracture and crack growth rate properties because of internal porosity, surface roughness and residual stress. In general, hotter build process results in more ductile microstructure than that of SLM, which is richer in martensite, strong but brittle.[17,19] Both heat treatment and HIP processes can significantly improve these properties.[21–23]

Table 1 Chemical compositions of the wires used for the present investigation

	Ti	Al	V	Fe	O	C	N	H	TOE	Y	Others
Grade 5	Bal.	6.14	3.96	0.18	0.14	0.02	0.011	0.001	<0.1	<0.001	<0.05
Grade 23	Bal.	6.18	4.02	0.099	0.052	0.021	0.0054	0.0016	<0.1	<0.0004	<0.03

So far, there is no published work on the fracture toughness and fatigue crack growth properties in the wire-fed AM Ti64. From a geometrical point of view, WAAM® can produce deposits of varying thickness by changing process parameters, such as the current, wire feed speed (WFS) or travel speed (TS). However, there is an upper limit with regards to the maximum width than can be produced with one bead only. If larger thicknesses are required, these can be achieved by laying beads next to each other in a parallel fashion, in which case the total width will be equal to the sum of the individual beads minus the overlap. Alternatively, the deposition head can be moved across the travel direction, in which case the total width will be roughly equal to the oscillation range. Each of these three deposition strategies will result in different thermal conditions and consequently different microstructures and residual stress variations.

This paper presents a series of experimental tests on the fracture and fatigue crack growth performance of Ti64 produced by the WAAM® process. The main objective is to obtain the fracture toughness and FCGR properties for this new material form to support its application in safety critical components that are based on the damage tolerance design criterion. Work reported in this paper are: (i) fracture toughness, and effects of build direction, deposition strategy and wire oxygen content, (ii) FCGR, and (iii) crack propagation behaviour in the proximity of the interface between WAAM® and wrought substrate. This is particularly relevant to the damage tolerant design at connections to the substrate: in some components produced by WAAM® the starting plate will be part of the final component, hence the properties at the interface, where the crack location and/or orientation with respect to the interface and loading direction can affect the crack growth behaviour, must be characterised.

EXPERIMENTAL

Deposition process

Straight walls were manufactured using a EWM T552 Tetrix Plasma power source. The motion was provided by a six-axis Fanuc Robot Arc Mate 120iB. Two types of aerospace 1.2 mm diameter Ti64 welding wire were used, grade 5 and 23, respectively; their chemical composition is shown in Table 1. The deposition parameters for the single, parallel and oscillation strategies are provided in Table 2 and their tool paths in Fig. 1. The single bead deposition strategy gave a deposit width of 8 mm, while the parallel and oscillation ones gave a width of 21 mm. Regardless of the strategy, shielding of the molten pool was provided by blowing BOC Pure Shield Argon at 8 l/min, and the plasma gas flow rate was 0.8 l/min; the inter-layer cooling time was 60 s. Deposition was performed in an inert atmosphere, inside a welding tent filled also with BOC Pure Shield Argon. In the tent, the achieved oxygen concentration, measured by an oxygen analyser, was generally between 200–600 ppm. The temperature of the room during welding was constant at 20 °C.

Table 2 WAAM® deposition parameters

Deposition strategy	Current (A)	WFS (m/min)	TS (mm/s)	Voltage (V)	Layer height (mm)
Single pass	145	2	4.5	19.9	1.25
Oscillation	150	2.3	4.75	20.1	1.50
Parallel	160	2.2	4.5	20.7	1.50

Specimens

The standard Compact Tension [C(T)] geometry (Fig. 2) was used for all three types of tests. Electron Discharge Machining (EDM) was used to extract the specimens from the walls and to cut the notch. Pre-cracking test was conducted to generate a crack from the notch root to ensure that the formal test is free of the notch root effect. Crack length generated at the end of pre-cracking test is recommended to be in the range of 0.45–0.55 W. In this work, the starting crack length was 35 mm, equal to 0.5 W.

Fracture toughness tests

Two different thicknesses were tested at 5 mm and 19 mm (these are the net thickness after surface machining from WAAM® deposit); both at the width dimension $W = 70$ mm, according to the ASTM E399 standard[27] for obtaining the apparent fracture toughness for a specified geometry. Two material orientations were tested, that is crack either in parallel or perpendicular to the WAAM® build direction. For the 5 mm thick material, four specimens were extracted from a WAAM® wall built on a flat substrate made of wrought Ti64 (Fig. 3a), that is two samples with the first orientation and other two with the second one.

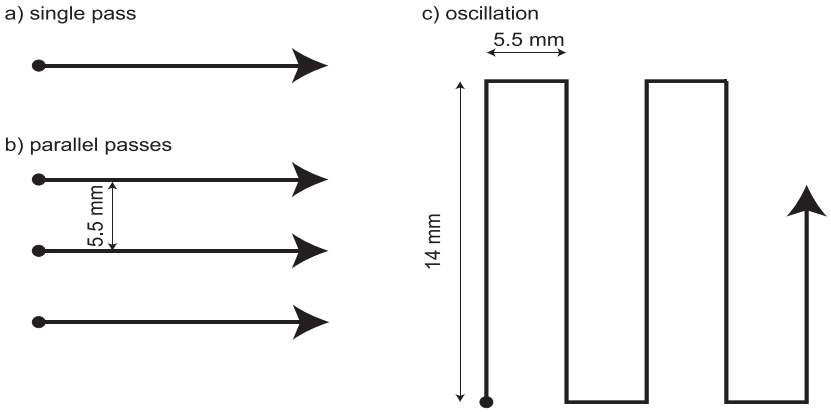

Fig. 1 Schematic of the tool path for the three deposition strategies (planar view).

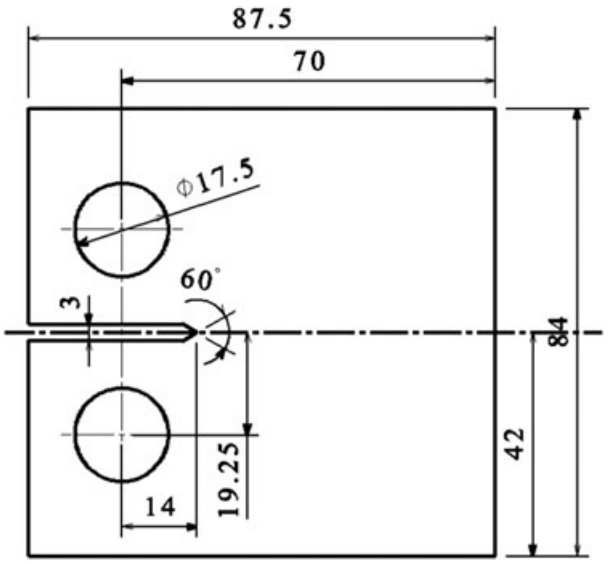

Fig. 2 Compact Tension (C(T)) specimen used for fracture toughness and fatigue crack growth rate tests. Dimensions: $W = 70$ for all thickness values reported in this paper. Thickness values refer to the finishing thickness (after surface machining). $B = 5$ mm for crack growth rate test in WAAM® alloy; $B = 6$ mm for crack growth rate test in WAAM®-wrought interface specimens; $B = 19$ mm for fracture toughness tests of all three different WAAM® deposition strategies (unit: mm).

The 19 mm thick test specimens are extracted from 21 mm thick deposited walls. After surface machining the thickness is 19 mm. Three straight walls were built.

- parallel deposition strategy using Ti64 grade 5;
- oscillation deposition strategy using Ti64 grade 5;
- parallel deposition strategy using Ti64 grade 23.

Fatigue crack propagation in WAAM® alloy

C(T) specimens extracted from a wall produced with the single bead deposition strategy were tested. Their dimensions were $W = 70$ mm and $B = 5$ mm. Two material orientations were tested, that is crack travelling along the layers, or across the layers. Tests and data reduction were conducted according to the ASTM E647 standard.[28]

Fatigue crack propagation near WAAM®-wrought interface

WAAM® was used to produce a straight wall along the edge of the starting plate, which was held vertically, using the single bead deposition strategy. The deposited walls measured 445 mm in length and 120 mm in height, so to produce effectively a structure which has half deposited material and half wrought. Five C(T) specimens were cut off from each wall representing five different crack location or orientation scenarios with respect to the WAAM®-substrate interface as shown in Fig. 3b. All specimens were 6 mm thick (after surface machining). Each test was repeated three times. The type A and C specimens have the interface aligned parallel to the applied load direction; in A, the initial crack started in the WAAM® portion; in C, the initial crack started in the wrought portion. The other three types all have the interface perpendicular to the applied load and the initial crack started at different material zones, that is on the interface (type B), or in the WAAM® portion (D), or in the wrought portion (E).

Testing

Fracture toughness testing

Fracture toughness test was conducted according to the ASTM E399 standard[27] using Instron machines of load capacity of 100 kN for the 19 mm thick specimens and 50 kN for the 5 mm thickness. Test was also conducted on 19 mm thick wrought Ti64 for comparison. A crack opening displacement (COD) gauge was used to measure the crack mouth displacement. The loading rate was 4 mm/min. Applied load versus crack opening displacement was measured and then used to determine the

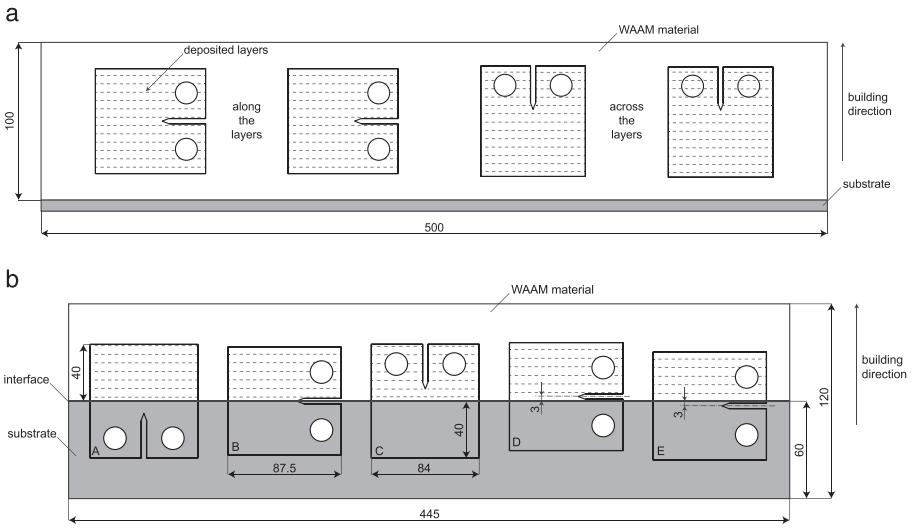

Fig. 3 a: Schematic of a WAAM® deposited wall and two orientations of specimens for fracture toughness tests. Four walls were made: for Grade 5 Ti64 using the single (8 mm thick), parallel (21 mm thick) and oscillation (21 mm thick) deposition strategies, and for Grade 23 using the parallel (21 mm thick) deposition strategy. Thickness values refer to the as-deposited condition, that is before surface machining (unit: mm). b Layout of five types of specimens on a WAAM®-substrate wall for fatigue crack growth tests (unit: mm). The thickness of the deposit was 8 mm. The final thickness of the C(T) specimens is 6 mm after machining. (Note: type B, D and E specimens have the same dimension as type A and C. Crack on B specimen is at the WAAM®-substrate interface; crack is 3 mm above the interface in D and 3 mm below the interface in E.)

maximum load at fracture P_{max} and the conditional value P_Q as shown in Fig. 4.

Fatigue crack growth testing

Pre-cracking test was conducted at the maximum applied load of 6 kN, load ratio 0.1 and loading frequency 10 Hz. Fatigue crack growth test was conducted at the same load ratio and frequency at the maximum applied load 5 kN. Crack length was measured by a travelling optical microscope of ×7 magnification. Crack growth rate as function of the SIF range was deduced from the measured crack length versus cycle number data using the 7-point polynomial method according to the ASTM E647 standard.[28]

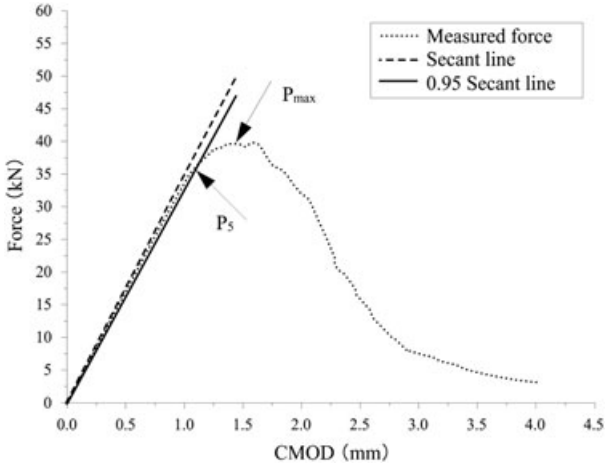

Fig. 4 Measured force versus crack mouth opening displacement in fracture toughness test, demonstrating the determination of P_Q. According to ASTM E399, this is the Type I case; thus $P_5 = P_Q$

Optical observation

Optical observation was performed after the tests at both macro and microscopic levels. Recommended procedures were followed for sample preparation, that is grinding, polishing and etching. Because the thickness of fatigue crack specimens was 6 mm, a 13 mm thick aluminium block was bonded to each of the OM samples to assist the polishing process.

RESULTS & DISCUSSION

Fracture toughness

First, conditional fracture toughness value (K_Q) was calculated for each test case according to ASTM E399[27] Values are presented in Table 3. To obtain the plane-strain fracture toughness (K_{IC}), test results must satisfy the following two requirements:

$$P_{max}/P_Q < 1.10 \tag{1}$$

$$2.5\left(\frac{K_Q}{\sigma_{ys}}\right)^2 < (W-a) \tag{2}$$

Table 3 K_Q and other relevant parameters in fracture toughness tests of WAAM® Ti-6Al-4V

		5 mm thick (nominal)		19 mm thick (nominal)		
Crack orientation		WAAM® Single	WAAM® Parallel grade 5	WAAM® Oscillated grade 5	WAAM® Parallel grade 23	Wrought (MA)
K_Q (MPa$\sqrt{m}$)	Across layers	81.8	73.2	82.1	96.2	76.9 (L-T)
	Along layers	73.9	70.9	74.3	95.1	
SD	Across layers	4.17	3.05	1.55	0.32	2.35
	Along layers	1.27	2.05	2.63	0.59	
P_{max} (kN)	Across layers	15.88	43.04	48.37	59.79	55.00
	Along layers	14.56	40.14	41.6	57.38	
P_Q (kN)	Across layers	11.15	40.92	47.42	53.28	41.27
	Along layers	10.15	36.84	39.64	49.34	
P_{max}/P_Q	Across layers	1.42	1.05	1.02	1.13	1.34
	Along layers	1.44	1.09	1.05	1.16	
a_c (mm)	Across layers	35	32.8	32.8	32.2	34.33
	Along layers	35	34.4	34.8	33.8	
W-a_c (mm)	Across layers	35	37.2	37.2	37.8	35.67
	Along layers	35	35.6	35.2	36.2	
B (mm)	Across layers	5.0	18.5	19.1	18.0	19.0
	Along layers	5.0	18.5	19.2	18.0	
$2.5(K_Q/\sigma_{ys})^2$ (mm)	Across layers	22.6	18.1	22.8	37.0	19.9 (L-T)
	Along layers	21.3	19.6	21.6	36.2	

Note: Width $W = 70$ mm for all specimens, B = thickness; 'MA' stands for 'Milled and Annealed' (wrought) condition; yield strengths used in calculations are: wrought (L-T): 950 ± 20 MPa [7]; WAAM® grade 5 wire (parallel, oscillated): 860 ± .3.8 MPa (along layers) [7], 800 ± 7.2 MPa (across layers) [7]; WAAM® grade 23 wire: 760 MPa [AMS B381-13] (used for both directions)

where P_{max} is the maximum load at fracture, P_Q a calculated maximum load based on the test measured load versus displacement relation according to ASTM E399. Values of yield strength (σ_{ys}) used in the calculation are given in Table 3.

An example of measured force versus displacement curve is shown in Fig. 4 with indication of the P_{max} and P_Q. Based on the calculated results from Eqs.[1] and,[2] which are also listed in Table 3, K_Q equals to K_{IC} for the 19 mm thick WAAM® and wrought materials (although the grade 23 wire specimens have slightly higher than the required P_{max}/P_Q ratio). For the wrought condition (19 mm thick), toughness measured in this study is 76.9 MPa$\sqrt{m}$. Published wrought Ti64 plane strain fracture toughness is in the order of 66 MPa$\sqrt{m}$.[16] WAAM® plane strain fracture toughness is higher than that of the wrought based on the 19 mm specimen test, or similar in the case of grade 5 wire with parallel deposit strategy. Figure 5 shows a comparison of all test results. Test of the 5 mm thick WAAM® material is not a valid K_{IC} test; hence, the measured fracture toughness is only valid for the specific thickness. In this case the elastic–plastic effect on toughness needs to be accounted, which is beyond the scope of this study.

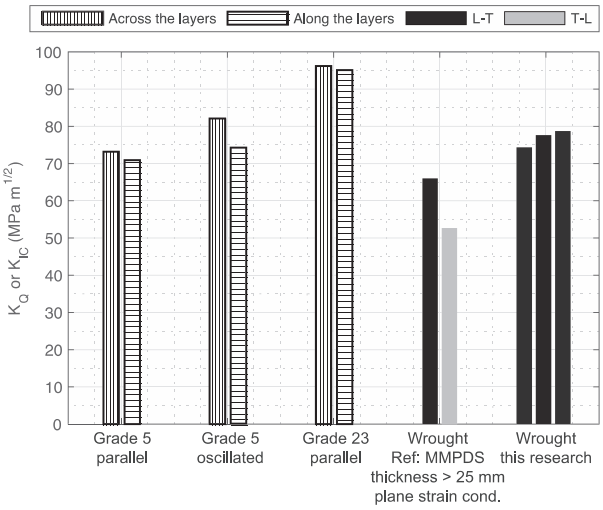

Fig. 5 Effect of build method, material orientation and wire oxygen content on fracture toughness of WAAM® Ti-6Al-4V and comparison with that of wrought condition (all have 19 mm thickness), and comparison with a reference plane-strain value (thickness > 25 mm).

Effect of thickness

As expected, K_Q of the thin specimen is greater than that of the thicker specimens. Note that only specimens cut from the thick wall produced with parallel deposition strategy are used for comparison with the 5 mm thickness, as it was built using the same torch movement direction and wire oxygen content as the thinner specimen. When the crack propagates across the layers, the toughness of the thinner specimen is 11.7% higher than the thicker specimen (81.8 versus 73.2 MPa$\sqrt{m}$). When the crack propagates along the layers, the thinner specimen is only 4% higher than the thicker specimen

(73.9 versus 70.9 MPa$\sqrt{m}$). However, these differences are not as great as one would expect for ductile materials having big difference in thickness (5 versus 19 mm).

Effect of testing orientation and anisotropy

The toughness of the crack propagating across the layers was 1–3% higher than that of the crack propagating along the layers, regardless of the thickness or deposition strategy. For the 19 mm thick specimens, and for both grade 5 and grade 23 alloys, K_Q across the layers was always higher than along the layers (Fig. 5). For grade 5 deposit produced using the oscillation strategy, K_Q across the layers was 9.5% higher than along the layers. For the deposits produced using the parallel strategy this difference is smaller; in fact, for grade 5 parallel deposit strategy K_Q across the layers was 3.1% higher than along the layers; and for grade 23 parallel strategy the difference was just 1.2%.

The direction-dependant difference is ascribed to the bands observed in the microstructure of all specimens thus far produced by WAAM® as discussed in.[3,11] The banding appearance is given by a systematic and repetitive variation in the size of the α lamellae along the build direction, that is across the layers. Work reported in[3,11] have full explanation of the origin and characteristics of such bands. Regarding the present research, as shown in Fig. 6, the Widmanstätten microstructure is much coarser at the top of a band than that at the bottom. According to,[29] fracture toughness increases when the α grain size increases in alloys with a Widmanstätten microstructure characteristic. When the crack propagated along the layers, it followed the preferential path given by the finer microstructure at the bottom of a band for most of its lifetime. On the contrary, when the crack propagated across the layers, the specimen had greater fracture resistance, hence higher toughness value, because of the continuous variation of the α lamellae size seen at its tip.

Effect of deposition strategy

The test results show that the specimens produced using the oscillation deposition strategy had higher fracture toughness than those produced using the parallel deposition strategy. Optical microscopy images (Fig. 7) showed an overall much coarser microstructure for the oscillation deposition strategy (Fig. 7a and b) compared with the parallel one (Fig. 7c and d), with α lamellae that were not only thicker but also grouped in colonies. This agrees with what reported previously for alloys with a Widmanstätten microstructure characteristic,[23] in which fracture toughness increases as the α lamellae width increases. This is confirmed also by Fig. 8, in which the microstructure at the crack interface is shown. Fig. 8a, which refers to the specimens produced with the oscillation deposition strategy, exhibits a much coarser microstructure than that of the parallel strategy (Fig. 8b and c). For a detailed image of a large α colony present at the crack interface of the specimens produced with the oscillation deposition strategy, please refer to the higher magnification optical microscopy image shown in Fig. 8b.

Effect of oxygen content

Published work shows that the oxygen element can change the mechanical properties, for example the yield strength and fracture toughness.[30,31] This study has shown that fracture toughness is indeed affected by the wire oxygen content; lower oxygen element results in increase in fracture toughness. However, both the grade 5 and grade 23 materials used in the present research satisfy the requirements of material standards. In particular, fracture toughness of grade 23 was 34% higher than that of grade 5 material, and was higher than value of wrought condition (discussed later). However, no apparent microstructural differences were observed between the grade 5 and grade 23 specimens produced with the same parallel

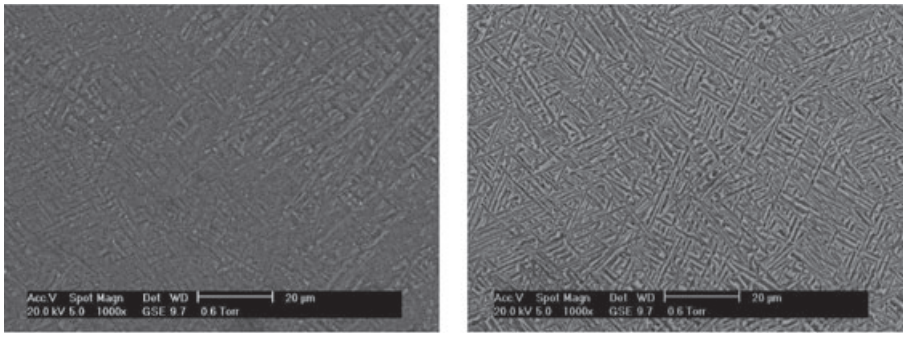

(a) (b)

Fig. 6 Changes in the size of the α observed in a linear deposit produced with the single bead deposition strategy: (a) fine structure at the bottom of a band, and (b) at the top of a band.

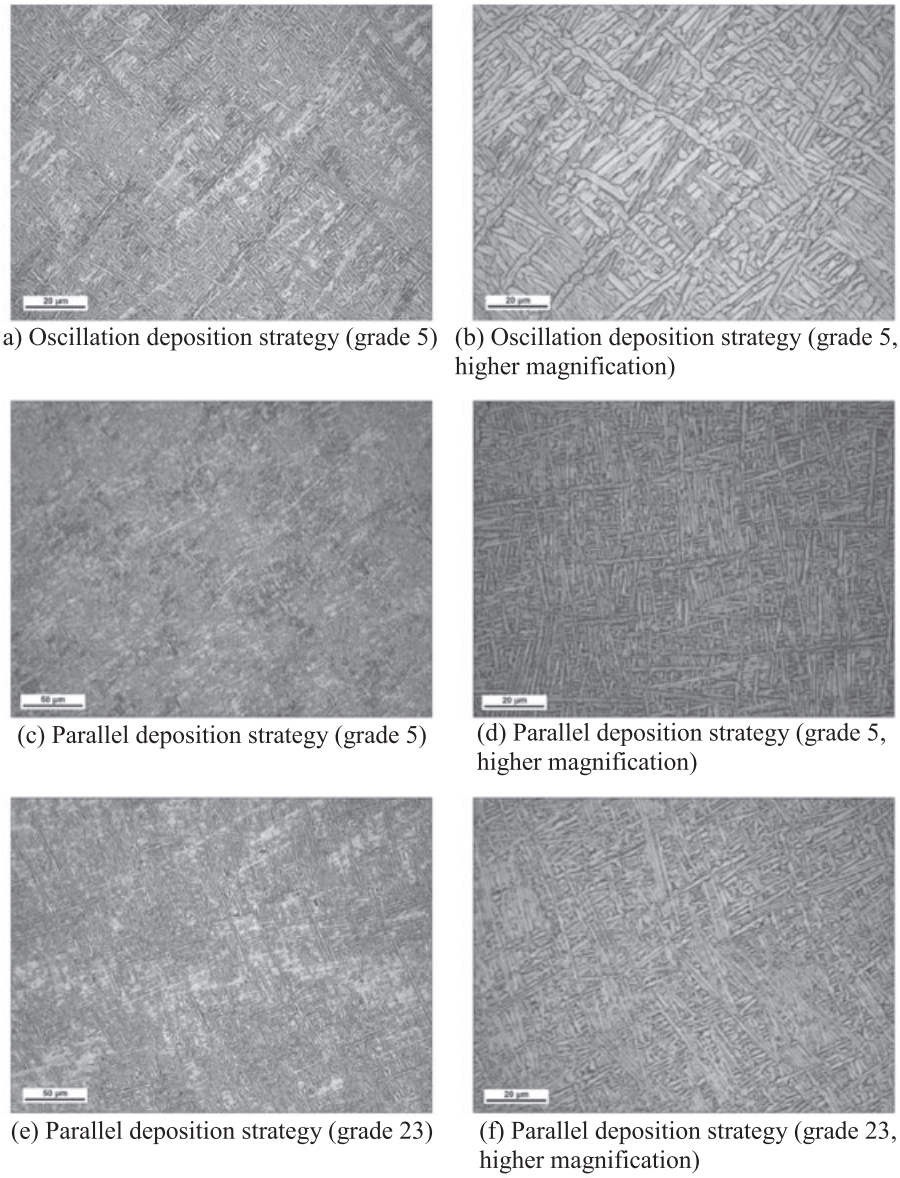

a) Oscillation deposition strategy (grade 5) (b) Oscillation deposition strategy (grade 5, higher magnification)

(c) Parallel deposition strategy (grade 5) (d) Parallel deposition strategy (grade 5, higher magnification)

(e) Parallel deposition strategy (grade 23) (f) Parallel deposition strategy (grade 23, higher magnification)

Fig. 7 Optical microscopy images showing the bulk of the deposited material.

deposition strategy (Fig. 7c and d versus Fig. 7e and f). It should be noted that grade 23 has lower static strength values.

Fatigue crack growth behaviour

Crack growth rates in wire + arc additive manufactured material

Fatigue crack growth rate in WAAM® grade 5 Ti64 as function of the SIF range is shown in Fig. 9a and compared with a wrought and a cast Ti64. Two observations can be made. First, FCGR in the wrought condition is greater than that in the WAAM® alloy, whereas the casting condition alloy has the slowest FCGR. Second, the specimen with crack propagating across the layers had slightly greater crack growth rate than that of the specimens with crack propagating along the layers. However, the difference is smaller than the scatter range allowed in fatigue tests. Therefore, the WAAM® material can be considered to have isotropic FCGR.

Crack growth rates in WAAM®-wrought interface specimens

Fatigue crack growth rates versus SIF range relation as presented in Fig. 9b is calculated from measured crack length versus load cycle relation using the 7-point polynomial method in the ASTM E647 standard. Following observations can be made.

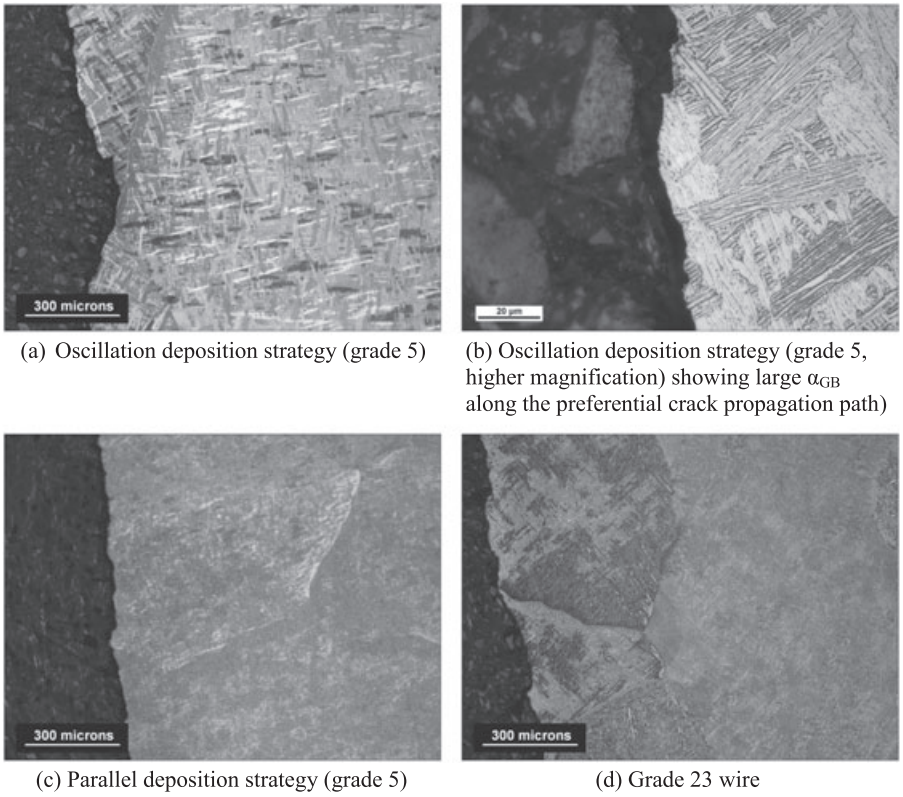

(a) Oscillation deposition strategy (grade 5)

(b) Oscillation deposition strategy (grade 5, higher magnification) showing large α_{GB} along the preferential crack propagation path)

(c) Parallel deposition strategy (grade 5)

(d) Grade 23 wire

Fig. 8 Optical microscopy images of the crack, highlighting the preferential path along the prior β grain boundaries.

Apart from type C specimen, FCGR is generally lower than the wrought condition, but greater than that of WAAM® alone material. However, all test data are within the normal scatter range.

For the specimens with the crack propagating across the layers orientation (type A and C), crack growth rates are noticeably greater than those with the crack propagating along the layers (B, D and E), indicating that crack growth resistance is weaker when crack is perpendicular to the build direction (i.e. along the layers). This may be attributed to the microstructure of the WAAM® Ti64 alloy that the interface between the β grains is weaker (crack propagates parallel with the β grains).

Type C has much greater crack growth rate than others, by 43–100% at higher K values owing to these factors: (i) crack started in WAAM® where there are tensile residual stress, although it only travelled a short distance in WAAM® (about 8–10 mm); (ii) crack subsequently went into the HAZ and substrate; crack growth rate in the latter is faster owing to the equiaxed microstructure.

Residual stresses in type A, B and C specimens were measured by the contour method and also calculated by FEM by inputting residual stresses in the original WAAM® wall (also measured by the contour method[12]) before extracting these C(T) specimens. Details can be found in.[12,32,33] As a summary, residual stresses are shown in Fig. 10. For type A specimen peak residual stress near the notch root of 100-130 MPa is measured (ignoring the highest stress calculated by FEA that is influenced by the stress concentration and mesh dependent at the notch root); the lowest stress is about −50 MPa. About 15 mm away from the notch root, residual stress is reduced to below 25 MPa. For type C specimen, peak stress of about 100 MPa is away from the notch root. Difference in stress distribution in A and C has caused different crack growth rate. For type B specimen, the peak stress is around 100 MPa that is quickly reduced to between −25 and 25 MPa. Although the magnitude of residual stresses in these specimens is relatively low comparing with the yield strength, their effect on crack growth should be considered because the SIF owing to residual stress is not negligible because of the crack tip stress intensity. Because the longitudinal residual stress is aligned with the applied load direction causing increase in the total SIF, greater crack growth rates in the A and C specimens are found. Crack growth rate in the type C is much faster than A, because the former had greater residual stress around the interface and the HAZ than that in A.[12] Type B has the slowest crack growth rate, suggesting that the WAAM®-wrought

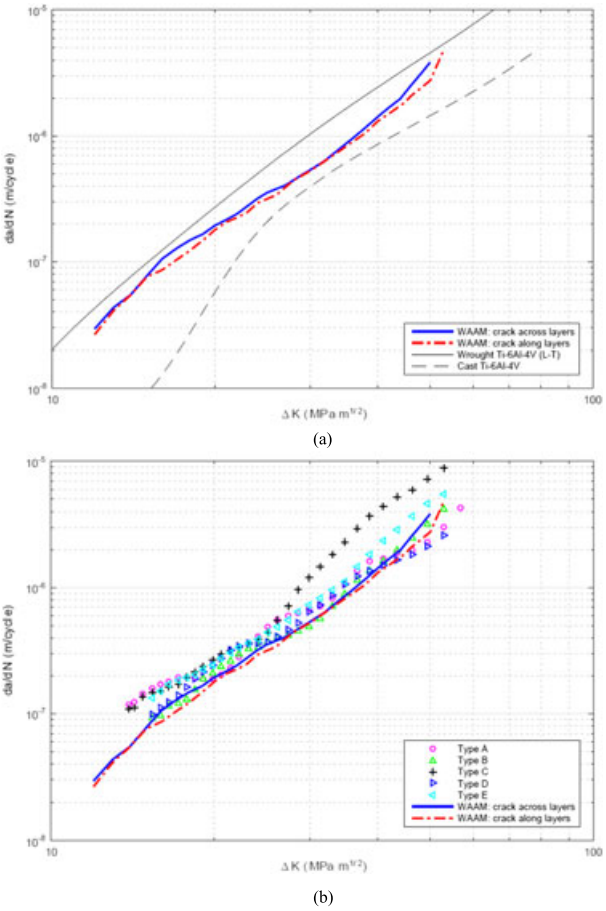

Fig. 9 Fatigue crack growth rate versus stress intensity factor range: (a) WAAM® material only and comparison with baseline wrought and cast conditions, (b) WAAM®-substrate interface and comparison with WAAM® material only.

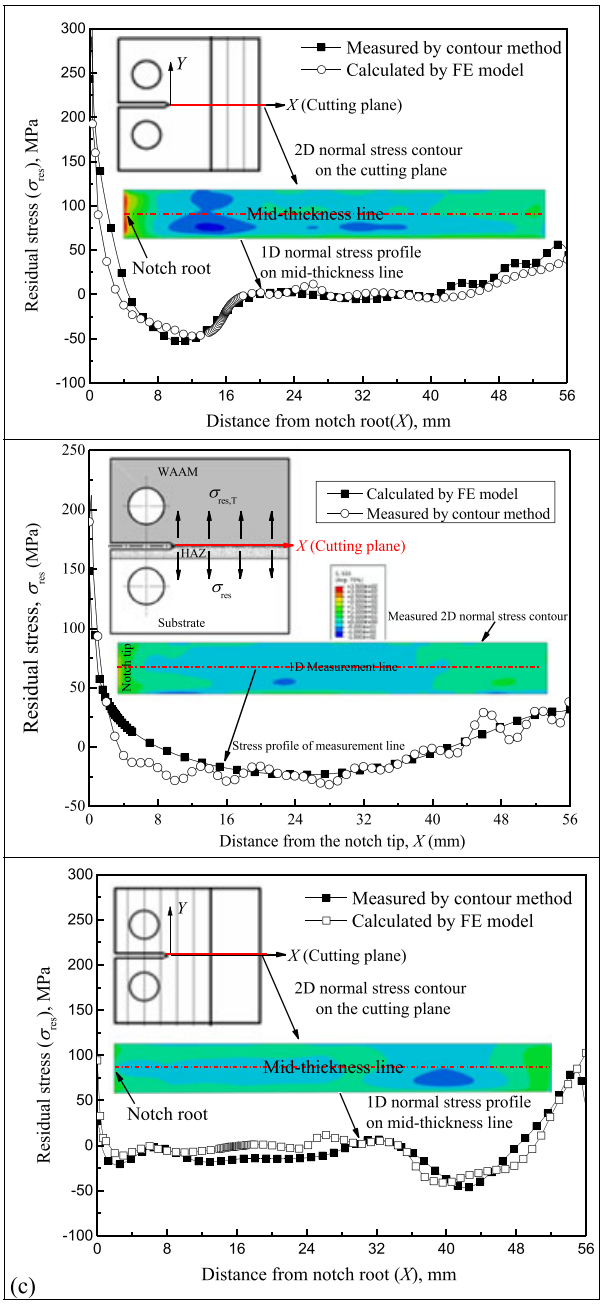

Fig. 10 Residual stresses in type A (a), B (b) and C (c) specimens. Residual stresses shown are in the direction of the applied load.[32,33]

interface has greater resistance to fatigue crack growth than that between the WAAM® interlayers (type D) and that of the substrate (type E). It should be noted that actual components made by WAAM® would be most likely stress-relieved prior to use. Therefore, the effect of residual stress will be null.

Crack trajectory

Macroscopic optical photographs show that crack in A and C specimens have kept a straight path during the crack propagation history (Fig. 11a and b). This is attributed to the symmetry in the applied load, residual stress and material properties.[12]

For the type B, D and E specimens, optical photographs show crack deviation from the initial crack plane (Fig. 11c, d and e). Mismatch of the bi-material properties and unsymmetric residual stress distribution are identified as the main causal mechanisms for the observed crack deviation.[30,32] It is noted that crack has the tendency to propagate into the substrate, even if the starting crack is in the WAAM® zone and about 3 mm from the interface (type D).

Fatigue crack morphology was investigated by optical microscope observation of polished and etched specimens. First, microstructure of the wrought substrate has finer and equiaxed structure, whereas the WAAM® alloy has a Widmanstätten microstructure. This is in

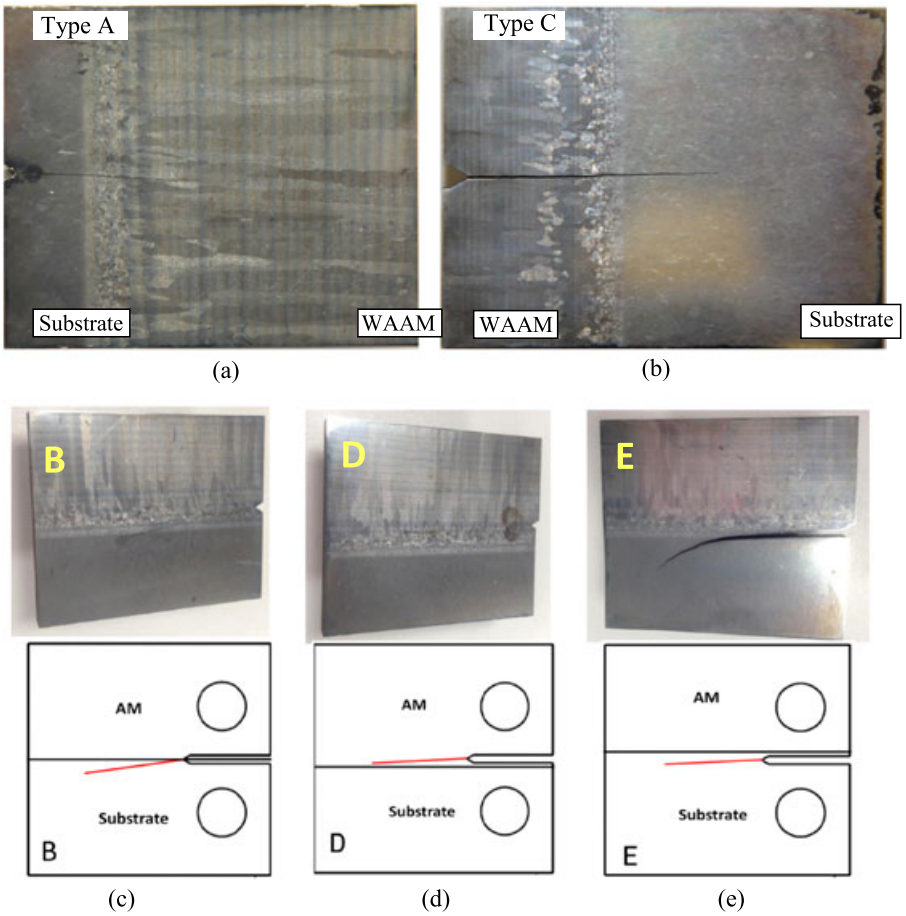

Fig. 11 Macroscopic photos showing the crack trajectory for each specimen type

agreement with the findings of titanium alloys fabricated by other additive manufacturing processes, for example SLM[34,35] and EBM.[36] Second, optical micrographs show that the crack path pattern varies as the crack propagates within different material zones.

Crack morphology of the type A specimen is presented in Fig. 12a and b. Crack path in the wrought portion was quite smooth and in a straight line (Fig. 12a), whereas in the WAAM® region it manifested a tortuous pattern (Fig. 12b). Similar results are also observed in type C specimen.[12]

Crack morphology of type B is shown in Fig. 12c and d. Initial crack was on the interface (re-melted zone or HAZ) manifesting a tortuous crack path (Fig. 12c). It subsequently propagated into the substrate alloy showing a smooth and straight path (Fig. 12d). Reasons identified for the observed crack deviation trend are: (i) both the residual stress field and material properties are unsymmetrical around the interface,[32] that is the crack is propagating in a bi-material system; (ii) the wrought alloy has less resistance to fatigue crack growth owing to its equiaxed grains; hence the crack has the tendency to grow into the wrought substrate.

Crack growth pattern in type D specimen (crack started in the WAAM® zone, 3 mm above the interface) is shown in Fig. 12e and f. In this case, the crack was transgranular through columnar prior β grains (Fig. 12e). Occasionally, the crack propagated along a prior β grain boundary; that explains the observed tortuous crack path in the type B, D and E (Fig. 12f).

Based on these microscopic observations, it is understood that the crack growth rate in type E is faster than that in the B and D specimens (Fig. 9b). This is partly because that the initial crack in E started from the wrought portion (3 mm from the interface), where the crack growth rate is much faster than that in the WAAM® area. The WAAM®-substrate interface seems to be a stronger weld bond with higher resistance to fatigue crack growth (specimen B) comparing with the WAAM® interlayer bond (D) and the wrought (E); this may explain the reason why the B specimen has the lowest crack growth rate among the three types.

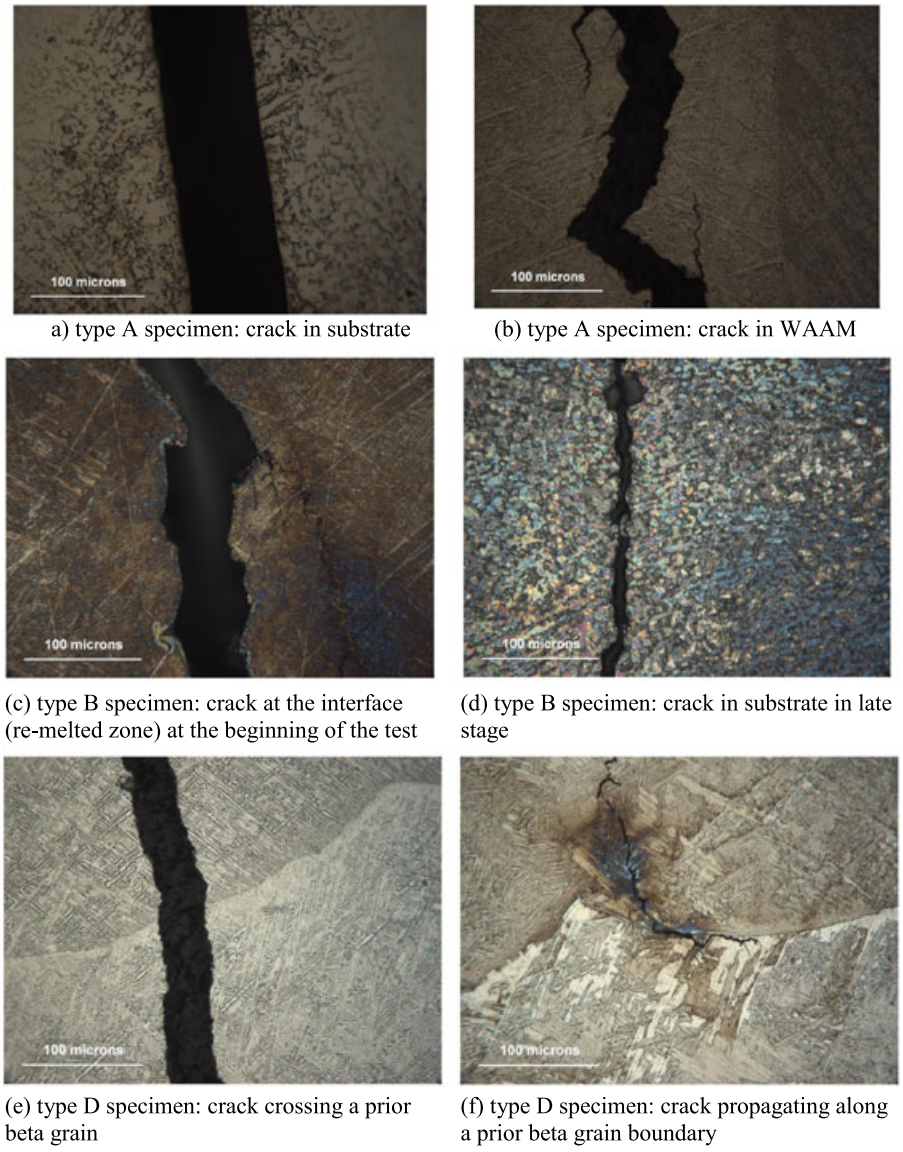

a) type A specimen: crack in substrate

(b) type A specimen: crack in WAAM

(c) type B specimen: crack at the interface (re-melted zone) at the beginning of the test

(d) type B specimen: crack in substrate in late stage

(e) type D specimen: crack crossing a prior beta grain

(f) type D specimen: crack propagating along a prior beta grain boundary

Fig. 12 Microscopic photos of crack growth patterns in type A, B and D specimens

CONCLUSIONS

For the Ti-6Al-4V specimens produced in this study by the WAAM® process, it was found that fracture toughness was comparable with or greater than properties of wrought Ti-6Al-4V, and FCGR was considerably lower than that in the wrought alloy. Therefore, for damage tolerance driven designs, WAAM® appears to be a viable candidate manufacturing process.This study also found that

- Grade 23 Ti-6Al-4V (lower oxygen content) has much greater fracture toughness (by 32%).
- Fracture toughness is direction dependent, i.e. it is slightly higher when crack propagates across the additive layers comparing to crack aligned with the layers. For grade 5 wire, the difference is within 3% (for the parallel deposition strategy) and 10% (for the oscillation deposition strategy).
- Fatigue crack growth rate is slightly faster when crack propagates across the layers comparing to crack propagating along the layers, but the difference is very small and within the range of data scatter.
- At the WAAM®-wrought interface, fatigue crack growth rate is generally greater than that in the pure WAAM® alloy. The difference is within the data scatter range. The only exception is when crack starts from the WAAM® part propagating toward the substrate; in this case, the crack growth rate is significantly faster.

Acknowledgements

The work was performed at Cranfield University with the support of the WAAMMat programme industrial partners (waammat.com). Financial support from the Engineering and Physical Sciences Research Council (Grant No EP/K029010/1) is acknowledged. Authors thank Emilie Lorant, Shijie Liu, Nick Hills and Dongni Wang for conducting part of the experiments, Dr Xianwei Liu and Andrew Dyer for their assistance on the microstructure examination. The data referred to in this article can be accessed at https://doi.org/10.17862/cranfield.rd.4042917.

REFERENCES

1 Williams, S. W., Martina, F. et al. (2015) Wire + air additive manufacture. *Mater Sci & Tech*, *IoM*, *DOI*. DOI:10.1179/1743284715Y.0000000073.
2 Frazier, W. E. (2012) Metal additive manufacturing: a review. *J. Mater. Eng. Perform.*, **23**, 1917–1928.
3 Martina, F., Mehnen, J., Williams, S. W. et al (2012) Investigation of the benefits of plasma deposition for the additive layer manufacture of Ti-6Al-4 V. *J. Mater. Process. Technol.*, **212**, 1377–86.
4 Wang, F., Williams, S. W. and Rush, M. (2011) Morphology investigation on direct current pulsed gas tungsten arc welded additive layer manufactured Ti6Al4V alloy. *Int. J. Adv. Manuf. Tech.*, **57**, 597–603.
5 Brandl, E., Baufeld, B., Leyens, C. et al (2010) Additive manufactured Ti-6Al-4 V using welding wire: comparison of laser and arc beam deposition and evaluation with respect to aerospace material specifications. *Phys. Procedia.*, **5**, 595–606.
6 Brandl, E., Palm, F., Michailov, V., Viehweger, B. and Leyens, C. (2011) Mechanical properties of additive manufactured titanium (Ti-6Al-4 V) blocks deposited by a solid-state laser and wire. *Materials & Design*, **32**, 4665–4675.
7 Wang, F., Williams, S., Colegrove, P. et al. (2013) Microstructure and mechanical properties of wire and arc additive manufactured Ti-6Al-4 V. *Metallurgical and Materials Transactions A.*, **44A**, 968–977.
8 Baufeld, B., Brandl, E. and Biest, O. (2011) Wire based additive layer manufacturing: comparison of microstructure and mechanical properties of Ti-6Al-4 V components fabricated by laser-beam deposition and shaped metal deposition. *J of Materials Processing Technology*, **21**, 1146–58.
9 Baufeld, B., Van der Biest, O. and Gault, R. (2010) Additive manufacturing of Ti-6Al-4 V components by shaped metal deposition: microstructure and mechanical properties. *Materials and Design*, **31**, S106–S111.
10 Brandl E, Leyens C, Palm F (2011). Mechanical properties of additive manufactured Ti-6Al-4 V using wire and powder based processes. In: Trends in Aerospace Manufacturing; 2009 International Conference, IoP Conf. Series: Materials Science and Engineering 26, 012004 doi:10.1088/1757-899X/26/1/ 012004, IOP Publishing Ltd.
11 Martina, F., Colegrove, P. A., Williams, S. W. and Meyer, J. (2015) Microstructure of interpass rolled wire + arc additive manufacturing Ti-6Al-4 V components. *Metallurgical and Materials Transactions A*, **46**, 6103–6118.
12 Zhang, J., Wang, X., Paddea, S. and Zhang, X. (2016) Fatigue crack propagation behaviour in wire + arc additive manufactured Ti-6Al-4 V: effects of microstructure and residual stress. *Materials & Design*, **90**, 551–561.
13 Ding, J., Colegrove, P., Mehnen, J., Williams, S. W., Wang, F. and Sequeira Almeida, P. (2013) A computationally efficient finite element model of wire and arc additive manufacture. *Int J Adv Manuf Technol*, **70**, 227–236.
14 Martina F, Roy MJ, Szost BA, Terzi S, Colegrove PA, Williams SW, Withers PJ, Meyer J, Hoffmann M (2016). Residual stress of as-deposited and interpass rolled wire + arc additive manufacturing Ti-6Al-4 V components. Materials science & technology, accepted 12 Jan 2016.
15 Szost, B., Terzi, S., Martina, F., Boisselier, D., Prytuliak, A., Pirling, T., Hofmann, M. and Jarvis, D. J. (2015) A comparative study of additive manufacturing techniques: residual stress and microstructural analysis of CLAD and WAAM printed Ti-6Al-4 V components. *Materials & Design*, **89**, 559–567.
16 Edwards, P., O'Conner, A. and Ramulu, M. (2013) Electron beam additive manufacturing of titanium components: properties & performance. *J Manufact Sci & Engng*, **135**, 061016/1–7.
17 Van Hooreweder, B., Moens, D., Boonen, R., Kruth, J.-P. and Sas, P. (2012) Analysis of fracture toughness and crack propagation of Ti-6Al-4 V produced by selective laser melting. *Advanced Engineering Materials*, **14**, 92–97.
18 Leuders, S., Thöne, M., Riemer, A., Niendorf, T., Tröster, T., Richard, H. A. and Maier, H. J. (2013) On the mechanical behaviour of titanium alloy TiAl6V4 manufactured by selective laser melting: fatigue resistance and crack growth performance. *Int J of Fatigue*, **48**, 300–307.
19 Edwards, P. and Ramulu, M. (2015) Effect of build direction on the fracture toughness and fatigue crack growth in selective laser melted Ti-6Al-4V. *Fatigue Fract Engng Mater Struct.*, **38**, 1228–1236.
20 Niendorf T (2015). TU Bergakademie Freiberg, Germany. Private Communications, 10 Sept 2015.
21 Caina, V., Thijs, L., Van Humbeeck, J., Van Hooreweder, B. and Knutsen, R. (2015) Crack propagation and fracture toughness of Ti6Al4V alloy produced byselective laser melting. *Additive Manufacturing*, **5**, 68–76.
22 Riemer A, Richard HA. Crack propagation in additive manufactured materials and structure. 21st European Conference on Fracture, ECF21, 20-24 June 2016, Catania, Italy. Published in *Procedia Structural Integrity*, **2**(2016) 1229–1236.
23 Riemer, A., Richard, H. A., Brugemann, J.-P. and Wesendahl, J.-N. (2015) Fatigue crack growth in additive manufactured productes. *Frattura ed Integrità Strutturale*, **34**, 437–446. DOI:10.3221/IGF-ESIS.34.49.
24 Zhai, Y., Lados, D. A., Brown, E. J. and Vigilante, G. N. (2016) Fatigue crack growth behavior and microstructural mechanisms in Ti-6Al-4 V manufactured by laser engineered net shaping. *Int J of Fatigue*, **93**, 51–63.
25 Scott-Emuakpor, O., Schwartz, J., George, T., Holycross, C., Cross, C. and Slater, J. (2015) Bending fatigue life characterisation of direct metal laser sintering nickel alloy 718. *Fatigue Fract Engng Mater Struct.*, **38**, 1105–1117.
26 Croccolo, D., De Agostinis, M., Fini, S., Olmi, G., Vranic, A. and Ciric-Kostic, S. (2016) Influence of the build orientation on the fatigue strength of EOS maraging steel produced by additive metal machine. *Fatigue Fract Engng Mater Struct*, **39**, 637–647.
27 ASTM E399 (2009) *Standard Test Method for Linear-Elastic Plane-Strain Fracture Toughness* K_{Ic} of Metallic Materials, Annual Book of ASTM Standards: Pennsylvania, US.

28 ASTM E647 (2013) *Standard Test Methods for Measurement of Fatigue Crack Growth Rates*, Annual Book of ASTM Standards: Pennsylvania, US.
29 Tsangarakis, N. (1983) On the dependence of fracture toughness on metallurgical factors. *Materials Science and Engineering*, **58**, 269–276.
30 Campbell FC (Ed.) (2012). Fatigue and fracture: understanding the basics. ASM International, 242.
31 Wessel, J. K. (2004) *Handbook of Advanced Materials: enabling new Designs*, John Wiley & Sons, pp. 292.
32 Zhang, J., Zhang, X., Wang, X., Ding, J., Traoré, Y., Paddea, S. and Williams, S. (2016) Fatigue crack path selection at the interface of wire + arc additive manufactured Ti-6Al-4V. *Materials & Design*, **104**, 365–375.
33 Zhang J, Chen B, Zhang X. n.d, Residual stress and its influence at the interface of wire + arc additive manufactured titanium alloys. Rare Metal Materials and Engineering, (in Chinese), accepted for publication.
34 Kelly, S. M. and Kampe, S. L. (2004) Microstructural evolution in laser-deposited multilayer Ti-6Al-4 V builds: part I. *Microstructural characterization. Metallurgical & Materials Transactions A*, **35**, 1861–1867.
35 Kelly, S. M. and Kampe, S. L. (2004) Microstructural evolution in laser-deposited multilayer Ti-6Al-4 V builds: part II. *Thermal modeling. Metallurgical & Materials Transactions A*, **35**, 1869–1879.
36 Taminger KM, Hafley RA (2006). Electron beam freeform fabrication for cost effective near-net shape manufacturing. NATO/RTOAVT-139 Specialists' meeting on cost effective manufacture via net shape processing, Amsterdam, the Netherlands, pp. 9-25

